

## Article

# Potential Utilization of Loess in Grouting Materials: Effects of Grinding Time and Calcination Temperature

Hao Bai, Kai Wang \*, Xiaoqiang Zhang, Yulong Jiang and Shiyu Zhang

School of Mining Engineering, Taiyuan University of Technology, Taiyuan 030024, China; baihao1070@link.tyut.edu.cn (H.B.); tyzxq2009@163.com (X.Z.); zhangshiyu@tyut.edu.cn (S.Z.)

\* Correspondence: wangkai@tyut.edu.cn

**Abstract:** There is a huge reservation of loess in the Shanxi mining area in China, which has great potential for preparing supplementary cementitious materials. Loess was modified via mechanical and thermal activation, and the pozzolanic activity was evaluated using an Inductively Coupled Plasma Optical Emission Spectrometer (ICP-OES). Moreover, the workability of grouting materials prepared using modified loess was assessed. The experimental results revealed that the number of ultrafine particles gradually increased with the grinding time, enhancing the grouting performance. The coordination number of Al decreased upon the breakage of the Al–O–Si bond post-calcination at 400 °C, 550 °C, 700 °C, and 850 °C. Moreover, the breaking of the Si–O covalent bond produced Si-phases, and the pozzolanic activity of loess increased. Furthermore, the modified loess was hydrated with different cement proportions. With increasing grinding time, the overall setting time increased until the longest time of 14.5 h and the fluidity of the slurry decreased until the lowest fluidity of 9.7 cm. However, the fluidity and setting time decreased with increasing calcination temperature. The lowest values were 12.03 cm and 10.05 h. With the increase in pozzolanic activity, more ettringite was produced via hydration, which enhanced the mechanical properties. The maximum strength of the hydrated loess after grinding for 20 min reached 16.5 MPa. The strength of the hydrated loess calcined at 850 °C reached 21 MPa. These experimental findings provide theoretical support for the practical application of loess in grouting.



**Citation:** Bai, H.; Wang, K.; Zhang, X.; Jiang, Y.; Zhang, S. Potential Utilization of Loess in Grouting Materials: Effects of Grinding Time and Calcination Temperature. *Minerals* **2024**, *14*, 490. <https://doi.org/10.3390/min14050490>

Academic Editors: Manuel Pozo Rodríguez, Francisco Franco and Michael G. Stamatakis

Received: 17 March 2024

Revised: 2 May 2024

Accepted: 4 May 2024

Published: 6 May 2024



**Copyright:** © 2024 by the authors. Licensee MDPI, Basel, Switzerland. This article is an open access article distributed under the terms and conditions of the Creative Commons Attribution (CC BY) license (<https://creativecommons.org/licenses/by/4.0/>).

**Keywords:** loess; mechanical activation; pozzolanic activity; supplementary cementitious materials; thermal activation

## 1. Introduction

The production of Portland cement causes considerable carbon emissions, and the replacement of cement clinkers with materials with pozzolanic activity can effectively reduce the environmental impact of cement-based materials. Some materials with low economic value require physical or chemical modification because of their extremely low pozzolanic activity. Recently, mechanical grinding has been frequently used as a physical modification method, improving the pozzolanic activity by changing the particle size, whereas chemical modification methods improve pozzolanic activity via high-temperature calcination, destroying the ordered structure. For example, adding natural pyrophyllite at 10%, 30%, and 50% had diverse effects on the properties of cement paste and mortar. The mechanical properties and hydration properties of cement paste were improved by the mechanical activation of natural pyrophyllite [1]. Mechanical–chemical activation affected the particle size distribution, morphology, and bulk and surface chemical structures of kaolinite and montmorillonite clays. Mechanical activation methods are effective in increasing the pozzolanic activity of 2:1 clay minerals (muscovite and montmorillonite) [2]. The pozzolanic activity of natural clay, fly ash (FA), metakaolin (MK), and quartz sand was evaluated using the strength activity index (SAI), Frattini test, and electrical conductivity test after mechano-chemical activation [3,4], and the pozzolanic activity and hydration properties

of feldspar, siliceous metal tailings, and quartz improved. The activity of pozzolanic ash increases with grinding time but reaches a limit [5–7]. The reaction kinetics, rheological properties, setting times, compressive strength, hydration products, and microstructure of the samples were studied by adding metakaolin with different particle sizes and dosages to modified FA cement [8]. The effects of mechanically activated mica and talc have been studied from the perspective of industrial applications [9]. For kaolin and white mica, with increasing grinding time, the particle size and crystallinity decrease, whereas the specific surface area and pozzolanic activity index increase. They can react with calcium hydroxide to form hydrated calcium silicate—a typical characteristic of the pozzolanic reaction [10,11]. Clay can be used as a supplementary cementitious material post-milling [12,13].

Moreover, calcined clays can be used as supplements to coal-based cementitious materials, such as slag. In addition, calcination as a means of pozzolanic activity enhancement is of great importance in the development of supplementary cementitious materials [14]. Supplementary cementitious materials were prepared using illite/chlorite (I/C) shale with a calcination window between 900 °C and 1000 °C. The results of Frattini tests showed that the materials exhibited pozzolanic activity 7 days post-calcination at 900 °C, whereas the SAI was the highest at day 28 for the clays calcined at 1000 °C [15]. The pozzolanic activity of gangue depends on the physical phase and structural changes of kaolinite during calcination. The highest pozzolanic activity was achieved when calcined at 800 °C for 2 h [16]. The strength and other properties of illite–montmorillonite clay as a geopolymer can be improved post-thermal and -alkali activation. Clays containing primarily illite were thermally activated between 550 °C and 950 °C [17]. When calcined materials with pozzolanic activity (marl, washed kaolin, coal kaolin, clay, and limestone) were added to silicate cement as supplementary cementitious materials, the physico-mechanical properties or pozzolanic activity considerably improved because of the reactive Al content and de-hydroxylated groups [18–21]. Metakaolin was synthesized by heating kaolinite in the temperature range of 550–950 °C for 6h. The metakaolin had good dehydroxylation properties. Natural kaolinite clay was calcined at 700 °C and its pozzolanic activity was evaluated using XRD and FTIR spectroscopy [22–24]. The calcined kaolin was analyzed using XRD, DTA, and FTIR. The mineralogy, de-hydroxylation, particle size, and crystallinity were closely related to the pozzolanic activity [25,26]. Moreover, the evolution of Si–Al in the gangue calcination process has been studied in terms of chemical and mineralogical properties [27]. Similarly, the mechanical properties of fired clay ceramics from 900 °C to 1200 °C at different heating rates were investigated [28].

The pozzolanic activity of materials can also be improved by combining multiple activation methods, such as mechano-thermal activation [29–33]. The active calcium produced by dissolving stone waste in a high-concentration alkaline slag solution can accelerate the hydration reaction. Moreover, an increase in the content of slag and alkaline solutions can improve the mechanical strength of a specimen [34]. To meet the requirements of engineering practices, the ratio of supplementary cementitious materials to silicate cement or other cementitious materials must be optimized based on the rheological properties of the slurry, setting time, compressive strength, and other aspects [35–38]. Results show that NaOH solution-cured loess depleted the quartz and feldspar in the loess, producing spherical, cubic, and small nanoscale particles of sodium aluminosilicate hydrate (N-A-S-H) and calcium (alumina) silicate hydrate (C-(A)-S-H) amorphous phase gels [39]. To assess the efficacy of bio-based materials, including calcium alginate (CA), xanthan gum (XA), cotton fibers (CO), and flax fibers (FA) in the treatment of loess, the improved soil's strength, disintegration, and water resistance were examined. Subsequently, an optimal amendment approach was determined, and dry–wet cycle tests and microscopic observations were performed [40].

Although mechanical–thermal activation improves pozzolanic activity, it has not been verified using loess materials. Loess is widely distributed in China and worldwide and is rich in clay content. However, the original loess is poor in activity, unstable in water, and collapsible. No one has improved the activity of loess by modifying it to improve its

utilization rate. The activation of loess as a supplementary cementitious material offers good prospects for development. In this study, loess was activated using mechanical grinding and high-temperature calcination. Particle size analysis and activity detection of the mechanically activated loess were performed. The high-temperature-calcined loess was detected using XRD and FTIR spectroscopy. In addition, the activated loess was mixed and hydrated with cement in different ratios for mobility, setting time, and compressive strength testing. Thermal analysis of the samples was performed post-hydration for 28 days, and the strength change mechanism was studied from the microscopic viewpoint.

## 2. Materials and Methods

### 2.1. Experimental Materials

The loess used in this paper originated from the Yitang coal mine regions. Raw loess was dried in a drying oven at 50 °C and then passed through a 1 mm sieve to remove large particles. The chemical and mineral compositions of the loess were measured using X-ray fluorescence spectroscopy (XRF) and X-ray diffraction (XRD) measurements, respectively. Using MDI JADE software in conjunction with the PDF database, based on the XRF results of the raw materials, the search range for elements was restricted to analyze the mineral composition of the raw materials. The XRD results shown in Figure 1 indicate that the main mineral phases of loess were quartz, kaolinite, calcite, microcline, muscovite, and chlorite. The composition of clay minerals in the loess was about 20%. Ordinary Portland cement (OPC) was employed as the main binder, and its chemical compositions and XRD patterns are also presented in Table 1 and Figure 1, respectively. As seen, the dominant minerals of the OPC were C<sub>2</sub>S, C<sub>3</sub>S, and calcite, respectively. Tap water was used for preparing fresh slurry, and deionized water was employed for the ion-leaching tests.

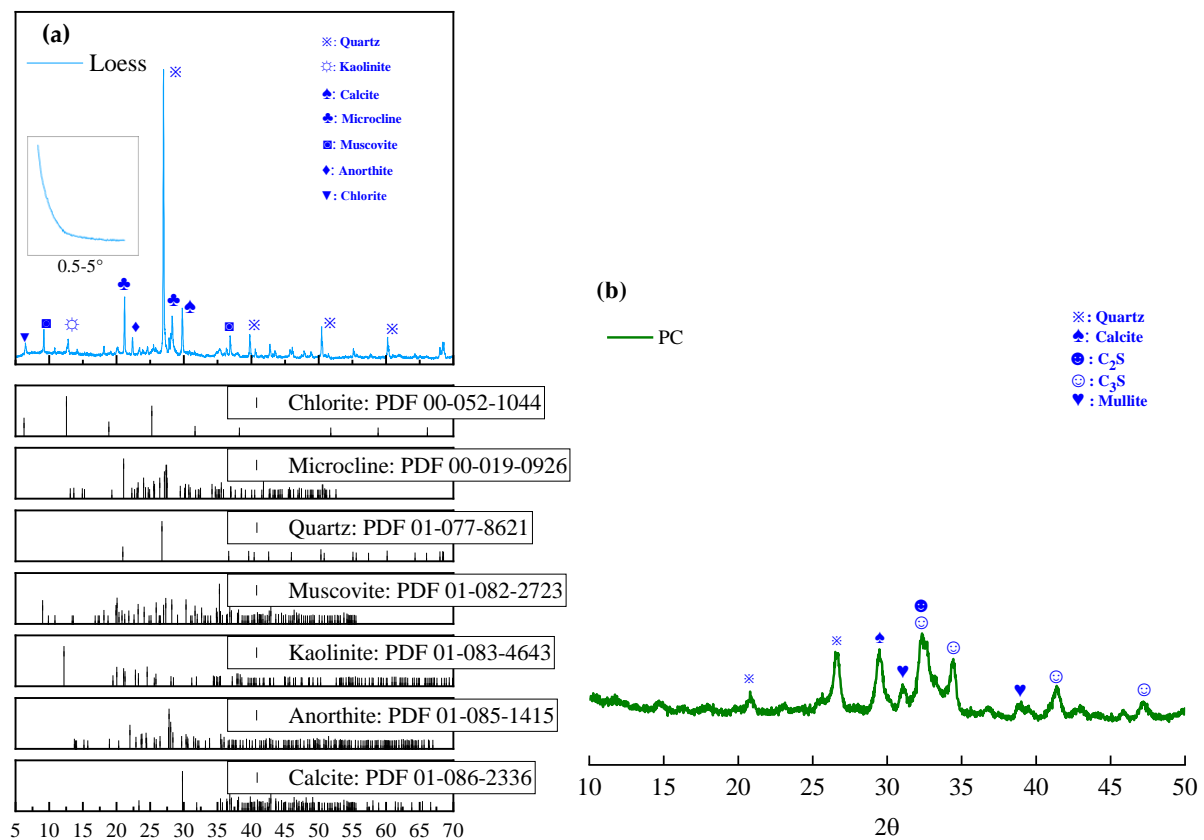


**Figure 1.** Mineral compositions of loess (a) and OPC (b). Quartz (SiO<sub>2</sub>), kaolinite (Al<sub>2</sub>Si<sub>2</sub>O<sub>5</sub>[OH]<sub>4</sub>), calcite (CaCO<sub>3</sub>), muscovite (KAl<sub>2</sub>(AlSi<sub>3</sub>O<sub>10</sub>)(OH)<sub>2</sub>), mullite (Al<sub>2</sub>SiO<sub>4</sub>).

**Table 1.** Chemical compositions of loess and OPC (%).

Oxides	OPC	Loess
CaO	65.544	11.663
SiO <sub>2</sub>	18.691	58.335
Al <sub>2</sub> O <sub>3</sub>	7.399	15.555
MgO	3.037	2.454
Fe <sub>2</sub> O <sub>3</sub>	2.597	6.047
Na <sub>2</sub> O	0.296	1.211
K <sub>2</sub> O	0.576	2.887
TiO <sub>2</sub>	0.604	1.101
P <sub>2</sub> O <sub>5</sub>	0.089	0.187
SO <sub>3</sub>	3.743	0.178
MnO	0.236	0.12
SrO	0.049	0.031
Cl	0.103	0.045
ZrO <sub>2</sub>	0.024	0.05

### 2.2. Grinding and Calcination of Loess

The screened loess was loaded into a ball mill for grinding. The ratio of the ball to the material was 1:1. The grinding time was varied (10, 20, 40, and 80 min). The loess with a grinding time of 20 min was loaded into a high-temperature-resistant Al<sub>2</sub>O<sub>3</sub> crucible for calcination. The upper limit of the calcination temperature was set to 400 °C, 550 °C, 700 °C, and 850 °C. The temperature was maintained for 1h after reaching the set value [30].

### 2.3. Sample Preparation

The modified loess was mixed with OPC to form a new grouting material. The detailed experimental program is shown in Table 2. The ratios of loess to OPC were 0.25, 0.54, and 1.0. The water–cement ratio was 1.0. After sufficient mixing, some of the fresh slurries were subjected to flow tests. The remaining slurries were poured into cylindrical plastic molds (height × diameter = 100 × 50 mm<sup>2</sup>). The specimens were remolded for 1 day and stored at 20 °C ± 2 °C and 95% ± 3% humidity.

**Table 2.** Experimental program used for mixing modified loess and cement in different proportions.

Sample Code	Mechanical Grinding of Loess (%)	Cement (%)	Water/Binder
G1	20 (G0)	80	1.0
G2	20 (G10)	80	1.0
G3	20 (G20)	80	1.0
G4	20 (G40)	80	1.0
G5	20 (G80)	80	1.0
G6	35 (G0)	65	1.0
G7	35 (G10)	65	1.0
G8	35 (G20)	65	1.0
G9	35 (G40)	65	1.0
G10	35 (G80)	65	1.0
G11	50 (G0)	50	1.0
G12	50 (G10)	50	1.0
G13	50 (G20)	50	1.0
G14	50 (G40)	50	1.0
G15	50 (G80)	50	1.0
Sample Code	Single-Calcined Loess (%)	Cement (%)	Water/Binder
C1	20 (C400)	80	1.0
C2	20 (C550)	80	1.0
C3	20 (C700)	80	1.0
C4	20 (C850)	80	1.0
C5	35 (C400)	65	1.0

Table 2. Cont.

C6	35 (C550)	65	1.0
C7	35 (C700)	65	1.0
C8	35 (C850)	65	1.0
C9	50 (C400)	50	1.0
C10	50 (C550)	50	1.0
C11	50 (C700)	50	1.0
C12	50 (C850)	50	1.0

#### 2.4. Methods

The modified loess samples were characterized using XRD, FTIR spectroscopy, and pozzolanic activity experiments. XRD tests were performed with a Panaco diffractometer (Panalytical X'pert Pro diffractometer). XRD measurements were performed from 5° to 50° (2θ) with a step interval and size of 0.02° and 2°/min, respectively. A Nexus 670 Infrared Spectrometer was used to measure the infrared spectra of powder samples. FTIR measurements were conducted in the absorption spectral range of 400–4000 cm<sup>-1</sup> with a sample/KBr ratio of 1/200–1/300. The raw materials were dispersed in absolute ethanol by ultrasound, and then the particle size distribution of the raw materials was measured by the Malvin Laser Particle Size Analyzer Mastersizer 3000. The particle size distribution (PSD) was measured using dynamic light scattering (DLS, Malvern). The instrument was equipped with a backscattering detector with a detection range of 0.1–11,000 nm. For pozzolanic activity testing, 4 g of dry co-combustion mixture and 100 mL of NaOH solution (1 mol/L) were placed into plastic test tubes and kept in a constant-temperature (20 °C) water bath oscillator for 7 days. The supernatant was filtered using 0.45 μm filter paper. The concentrations of Si<sup>4+</sup> and Al<sup>3+</sup> in the filtrate were determined using inductively coupled plasma emission spectrometry (ICP-OES) [32].

The practicality of the new grouting material was evaluated by measuring its setting time, fluidity, and strength. The Vickers apparatus used a priming needle of 50 ± 1 mm, a final needle of 30 ± 1 mm, a truncated cone test mold with upper and lower diameters of 65 ± 0.5 mm and 75 ± 0.5 mm, respectively, and a depth of 40 ± 0.2 mm. The setup used for the fluidity test had an upper diameter, a lower diameter, and a height of 50, 100, and 150 mm, respectively. Unconfined compressive strength (UCS) tests were performed with a loading capacity of 50 kN and a loading rate of 1 mm/min. The ASTM C39/C39-18 standard was followed. The hydration process of a new type of grouting material was studied by the thermogravimetric (TG) method with a STA409PC isothermal calorimeter (Germany) in a high purity N<sub>2</sub> environment at a temperature range of 30 °C to 1000 °C and a heating rate of 15 °C [41]. The contents of chemically bound water (CBW), CH, and CaCO<sub>3</sub> contained in blended binders with different hydration times could be obtained, and the calculation formula can be expressed as follows:

$$CBW = \frac{M_{50} - M_{550}}{M_{550}} \cdot 100\% \quad (1)$$

$$CH = \frac{M_{400} - M_{550}}{M_{550}} \cdot 100\% \cdot \frac{74}{18} \quad (2)$$

$$CH = \frac{M_{900} - M_{550}}{M_{900}} \cdot 100\% \cdot \frac{100}{44} \quad (3)$$

### 3. Results and Discussion

#### 3.1. Grinding Modification

##### 3.1.1. Particle Size Analysis

D<sub>10</sub>, D<sub>30</sub>, D<sub>50</sub>, D<sub>60</sub>, and D<sub>90</sub> represent the corresponding grain sizes when the cumulative loess volume fraction reached 10%, 30%, 50%, 60%, and 90%, respectively (Table 3, Figure 2). The particle size of the loess decreased with increasing grinding time, and the

proportion of ultrafine particles increased. The particle size  $D_{50}$  of the loess ground for 40 min was larger than that of the loess ground for 20 min owing to the agglomeration of ultrafine particles, resulting in an error in the test.  $C_u$  is the coefficient of inhomogeneity that reacted with the range of distribution of soil particles on the grain size distribution curve. If the coefficient of inhomogeneity was  $>5$ , this indicated that the soil had enough fine particles to fill the gap between coarse particles and make the soil dense.  $C_c$  is the curvature coefficient, which describes the smoothness of the gradation curve. When the curvature coefficient was 1–3, the gradation was considered sufficient. The calculation of the particle characteristics of loess with different grinding times showed that the ground loess had a good PSD, indicating that it was suitable as an aggregate or admixture for the preparation of grouting materials [42,43].

**Table 3.** Characteristic parameters of the particle size of fine loess.

Parameterization	G0	G10	G20	G40	G80
$D_{10}$ ( $\mu\text{m}$ )	15.89	2.24	1.78	1.59	1.42
$D_{30}$ ( $\mu\text{m}$ )	35.57	10.02	7.96	7.10	4.48
$D_{50}$ ( $\mu\text{m}$ )	50.24	22.44	17.83	20.00	12.62
$D_{60}$ ( $\mu\text{m}$ )	56.37	28.25	25.18	28.25	17.83
$D_{90}$ ( $\mu\text{m}$ )	112.47	63.25	56.37	70.96	44.77
$C_u = D_{60}/D_{10}$	3.55	12.59	14.13	17.78	12.59
$C_c = D_{30}^2/D_{60} \times D_{10}$	1.41	1.58	1.41	1.12	0.79
$U_g = (D_{90} - D_{60})/D_{50}$	1.12	1.56	1.75	2.14	2.14

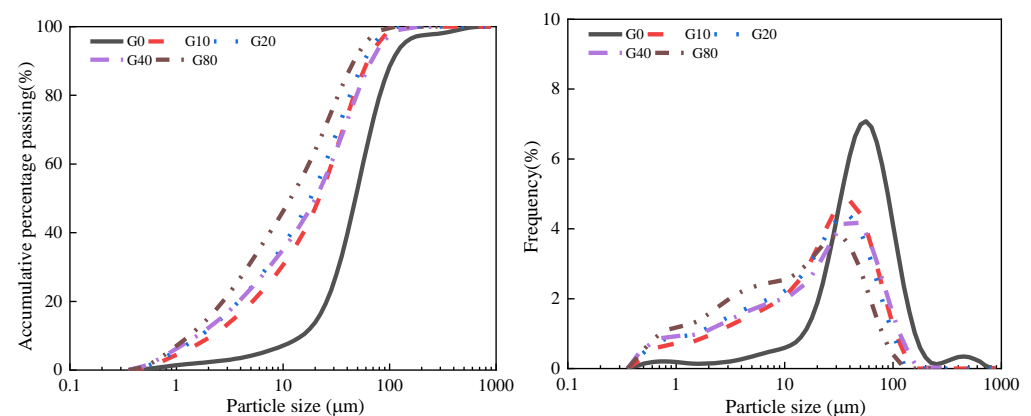


**Figure 2.** Particle size distribution of finely ground loess.

### 3.1.2. Pozzolanic Activity Analysis

The relationship between silicon and aluminum dissolution and the activity of activated loess was studied by the alkali dissolution method. There was a good correlation between the amount of  $\text{Si}^{4+}$  and  $\text{Al}^{3+}$  dissolved in various activated loess samples and their pozzolanic activity [44]. The ionic leaching concentration data for Si and Al in loess mixed in 1 mol/L NaOH solution at different grinding times are shown in Figure 3. The leachability of Si and Al increased with increasing grinding time. For example, the leaching concentrations of Si and Al in the loess material were 1.91 and 1.04 mg/L, respectively. As the grinding time increased from 10 to 80 min, the leaching concentrations of Si and Al increased from 2.63 to 4.55 mg/L and 1.29 to 2.04 mg/L, respectively. The effect of fine grinding was mainly emphasized in two aspects. First, grinding increased the specific surface area of the loess. When solid particles were dispersed in the NaOH solution, the contact points of  $\text{Na}^+$  and  $\text{OH}^-$  with solid particles increased. Thus, the probability of the breakage of Si–O and Al–O covalent bonds and subsequently the leachability of Si and Al increased. Second, the physico-mechanical action destroyed the internal structure of highly crystalline loess and increased the contact points of the alkaline reaction and the degree of disorder of Si and Al, thereby increasing the leachability of Si and Al. The trends of Si

and Al leaching concentrations and grinding times showed that the mechanical activation efficiency decreased with increasing grinding time [17,45].

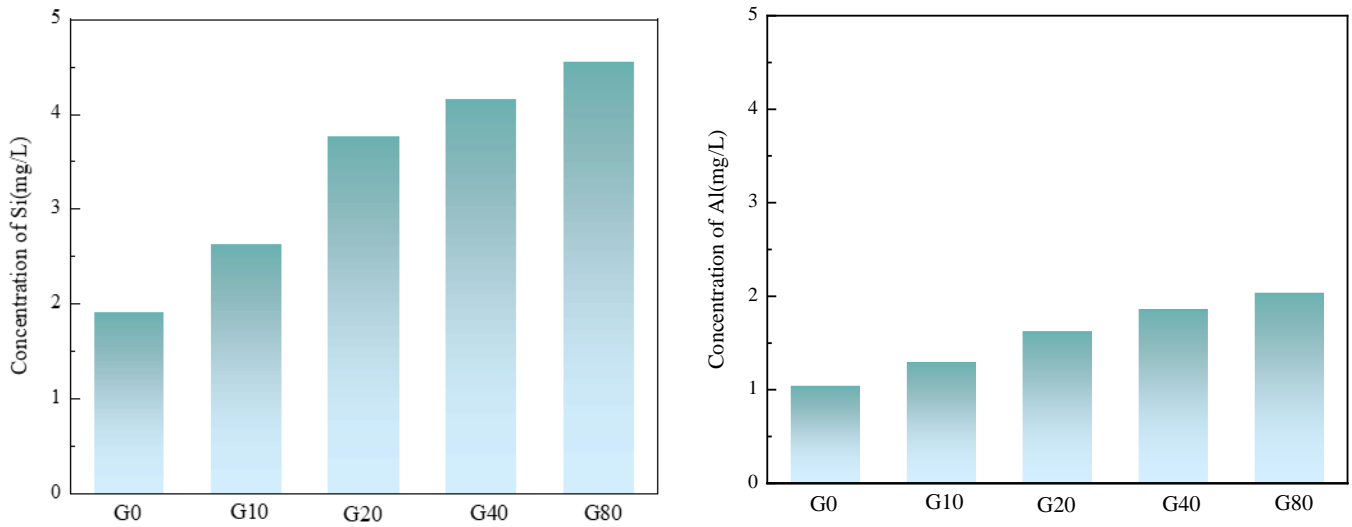


Figure 3. Concentrations of Si and Al leaching ions in ground loess.

### 3.2. Calcination Modification

#### 3.2.1. Mineral Phase Analysis

From the XRD phase analysis of the raw loess material, the loess mainly contained quartz, kaolinite, calcite, microcline, and muscovite. After high-temperature calcination, the XRD phases considerably changed (Figure 4) [18].

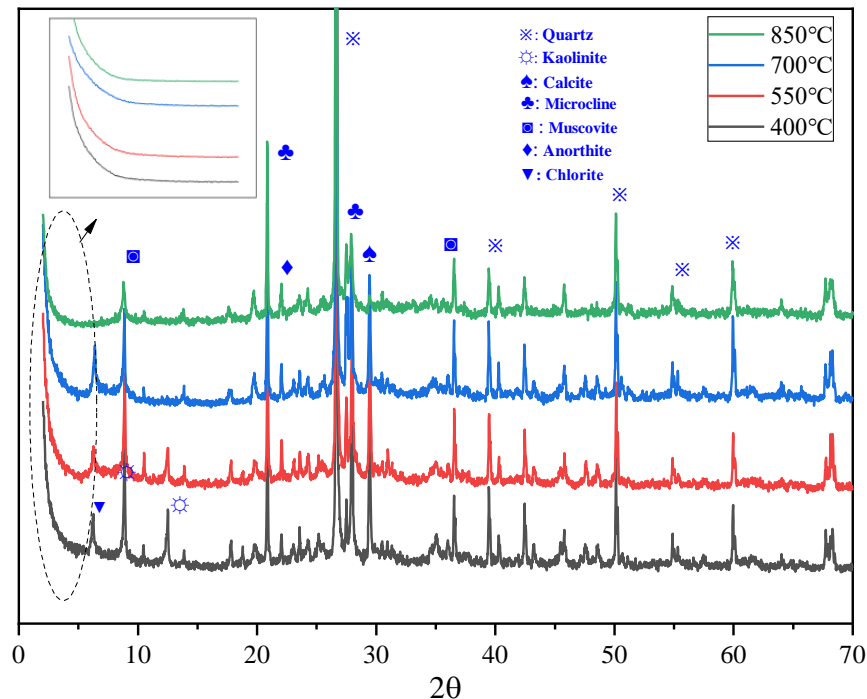


Figure 4. XRD phases of loess after single calcination at different temperatures.

When the calcination temperature was 400 °C, the peak intensity of kaolinite and other clay minerals was obvious. This stage was primarily the free water emanation stage with weak mineral binding. When the calcination temperature was increased to 550 °C, a slight attenuation was observed for the peak intensity of kaolinite and other

clay minerals, indicating that some poorly crystallized clay minerals lost interlayer water (hydroxyl) and that initial mineral morphology transformation occurred. When the calcination temperature was increased to 700 °C, the diffraction peaks of the kaolinite almost disappeared, indicating that the hydroxyl groups of the kaolinite were almost completely destroyed at this calcination temperature. During this time, the diffraction peak intensities of calcite and muscovite weakened. When the calcination temperature was increased to 850 °C, the peak intensities of muscovite and chlorite considerably decreased. When the calcination temperature increased from 400 °C to 850 °C, the relative peak intensity of quartz increased because of the dense crystalline structure and there was almost no phase transition [46].

### 3.2.2. Pozzolanic Activity Analysis

From the ionic leaching concentration data of Si and Al in a 1 mol/L NaOH solution of a single thermally activated loess sample (Figure 5), the leachability of Si and Al was remarkably enhanced post-calcination. For example, the leaching concentrations of Si and Al in the calcined raw loess materials were 3.96 and 1.75 mg/L, respectively. The leaching concentration of Si increased from 4.23 mg/L to 11.24 mg/L and that of Al from 1.91 mg/L to 7.91 mg/L when the calcination temperature increased to 400 °C–850 °C. The highest leaching concentrations of Si and Al were obtained at approximately 700 °C. During this time, clay minerals such as kaolinite lost their hydroxyl groups to produce amorphous Si and Al and released more Si and Al under the action of Na<sup>+</sup> and OH<sup>-</sup>. The change in Al leachability decreased when the calcination temperature increased from 700 °C to 850 °C owing to the re-crystallization of Al-containing minerals [14,47].

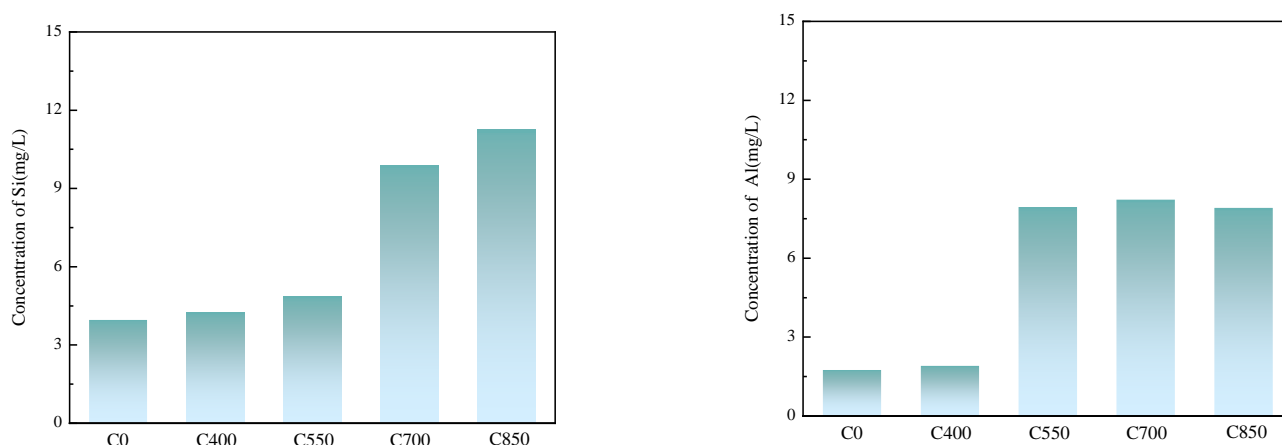


**Figure 5.** Dissolution characteristics of Si<sup>4+</sup> and Al<sup>3+</sup> ions in single-calcined loess at different temperatures.

### 3.2.3. FTIR Analysis

The vibrations of free water hydroxyl groups and mineral hydroxyl groups were distributed around 3400 cm<sup>-1</sup> and 3600 cm<sup>-1</sup> (Figure 6). The peak strength of the absorption band at 400 °C and 550 °C was larger than that at 700 °C and 850 °C. This indicated that there was still a large amount of chemically bound water in the calcined loess. The peak of the absorption bands became flat when the calcination temperature reached 700 °C. However, the absorption bands tended to flatten out when the calcination temperature reached 850 °C, indicating that at 700 °C, kaolinite minerals shed internal and external hydroxyl groups to transform into metakaolinite. The intensity of the hydroxyl absorption bands was greatly weakened. This was consistent with the results of the XRD experiments shown in Figure 4 [48].

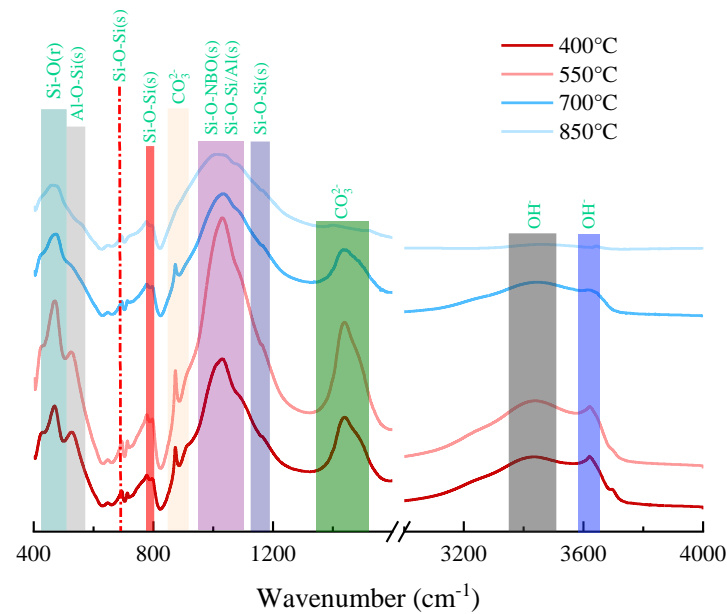


**Figure 6.** FTIR spectra of single-calcined loess at different temperatures.

The vibration at  $\sim 500\text{ cm}^{-1}$  in the spectra corresponded to the stretching vibration of the Al–O–Si chemical bond. The intensity of the spectral absorption bands gradually decreased as the calcination temperature increased from  $400\text{ }^{\circ}\text{C}$  to  $550\text{ }^{\circ}\text{C}$ . The absorption bands disappeared at  $700\text{ }^{\circ}\text{C}$ , indicating the destruction of the Al–O–Si chemical bond. During this time, Si atoms substituted for the Al atoms in the octahedron to form an unstable structure. Consequently, the ligand number of Al decreased and the pozzolanic activity increased. When the calcination temperature reached  $850\text{ }^{\circ}\text{C}$ , there was no further change in the spectra of the Al–O–Si absorption bands, indicating that the coordination of Al reached a stable state. The spectral bands in the range of  $400\text{--}500\text{ cm}^{-1}$  were the rocking vibrations of the Si–O bonds in the  $\text{SiO}_4$  tetrahedra, where the sharpness of the peaks decreased and the peak shoulders gradually widened. This indicated that the destruction of the covalent bonding of Si–O at high temperatures generated pozzolanic activity. The spectral bands at  $\sim 800\text{ cm}^{-1}$  and  $\sim 1200\text{ cm}^{-1}$  originated from the symmetric stretching vibrations of the Si–O–Si bonds, and their shapes barely changed. This implied that the quartz mineral phases remained unchanged upon calcination below  $850\text{ }^{\circ}\text{C}$ . This experimental phenomenon was consistent with the XRD results. The spectral bands at  $\sim 900\text{ cm}^{-1}$  and  $\sim 1400\text{ cm}^{-1}$  corresponded to all the anion vibrations in  $\text{CO}_3^{2-}$ . The intensities of the spectral bands slightly changed when the calcination temperature increased from  $400\text{ }^{\circ}\text{C}$  to  $700\text{ }^{\circ}\text{C}$ . However, they decreased sharply at  $850\text{ }^{\circ}\text{C}$ , suggesting that carbonate decomposed to a certain degree at  $850\text{ }^{\circ}\text{C}$ . The peak at  $\sim 1000\text{ cm}^{-1}$  was caused by the asymmetric stretching vibration of Si–O–NBO (non-bridging oxygen) and Si–O–Si/Al. The sharp decrease in the spectral band peaks and the gradual broadening of the two shoulders of the peaks indicated a complex change in the physical phase, which primarily included the substitution of positive ions, such as  $\text{Na}^+$ ,  $\text{K}^+$ , and  $\text{Ca}^{2+}$ , to form a non-bridging oxygen structure for Si–O [19,49].

### 3.3. Workability of Novel Grouting Materials

#### 3.3.1. Setting Time

Figure 7 shows the initial and final setting times of the grout prepared from loess with different mechanical activation times. When the dosage of the mechanically ground loess was 20%, the initial and final setting times appeared to first decrease and then increase. Post-grinding, the hydration activity of loess increased. The initial hydration rate was accelerated compared with that of the raw loess, and the setting time was reduced. With increasing grinding time, the ultra-fine particles in the loess increased. The hydration

reaction did not occur, and suspending the state existing in the pore solution was easy. Consequently, the removal of pore water was slowed and the setting time was increased. When the dosage of the mechanically ground loess was 35% and 50%, the initial and final setting times increased. For example, for a G0–G80 dosage of 35%, the initial coagulation time of the slurry increased from 9.24 h to 11.13 h. The final coagulation time increased from 11.20 h to 13.25 h. When the dosage of the mechanically milled loess was increased to 35% and 50%, the gain effect of the activity enhancement to accelerate the coagulation of the slurry was less than that of the increase in ultrafine particles to prevent free water exclusion, resulting in the slowed coagulation effect. Thus, the coagulation time was prolonged [50,51].

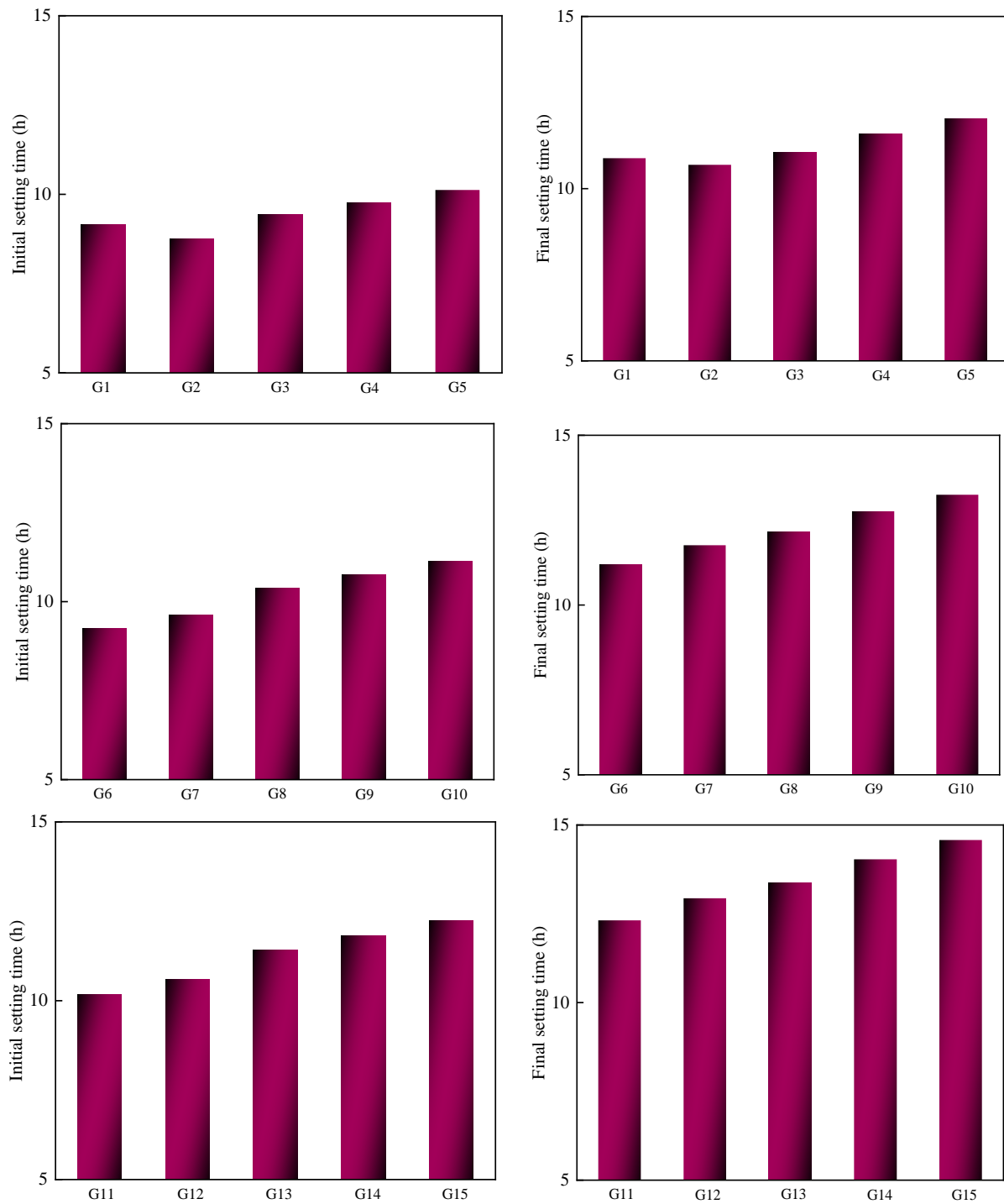


Figure 7. Setting times of mechanically activated loess-prepared grouting fluids.

The initial and final setting times of the slurry prepared using different dosages of single heat-activated loess are shown in Figure 8. Regardless of the dosage of the single heat-activated loess, the initial and final setting times of the slurry decreased with increasing calcination temperature. For example, with 20% C1–C4 doping, the initial and final setting times of the slurry were shortened from 9.37 h to 8.26 h and from 11.19 h to 10.05 h, respectively. After the calcination of loess, the hydration activity was partially improved. Increasing the temperature further improved the pozzolanic activity, accelerated the initial hydration rate, and reduced the setting time. When the content of loess increased, the setting time increased because the activity of single-calcined loess was lower than that of the cement, slowing down the hydration of the cementitious system and increasing the setting time [52,53].

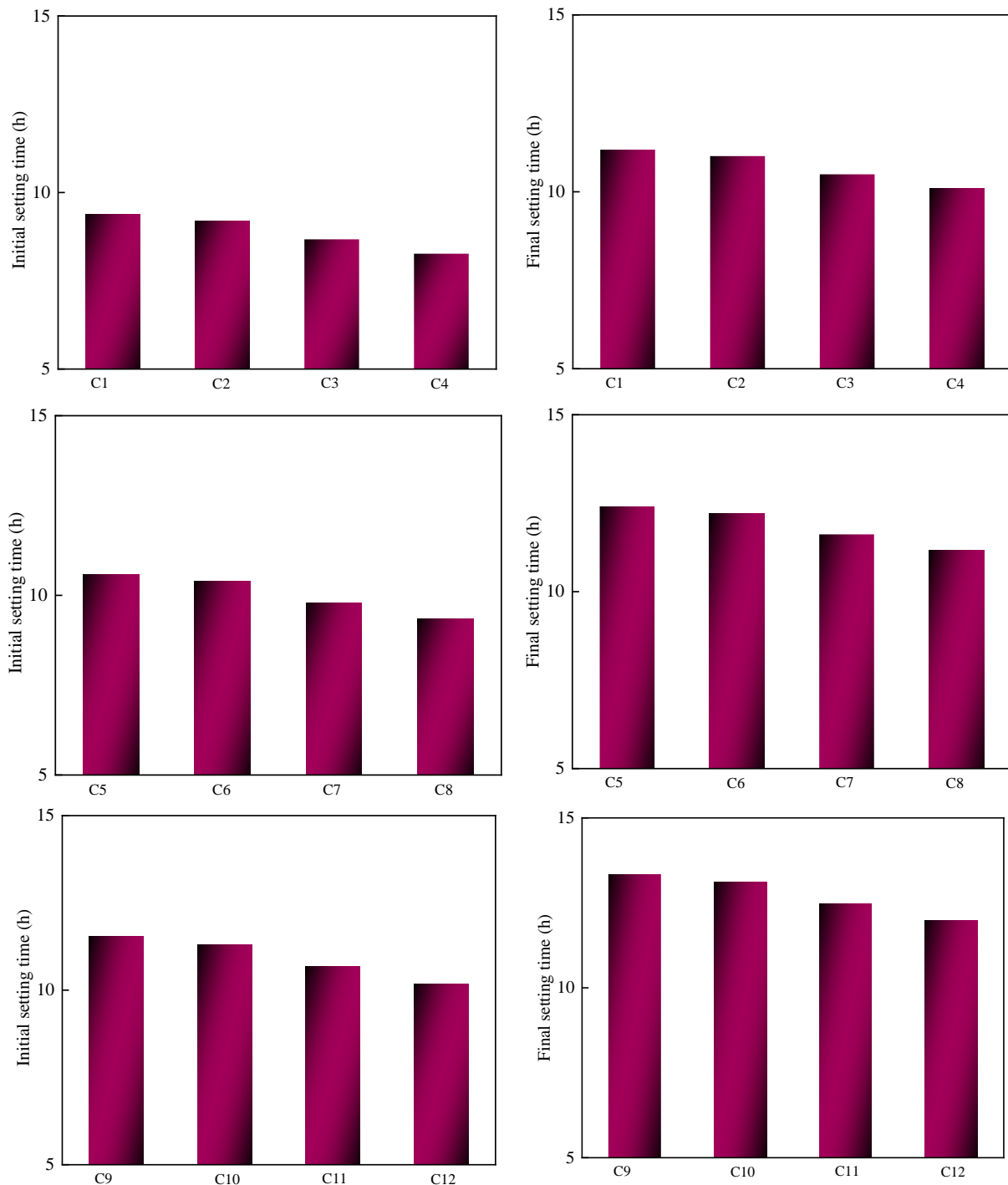
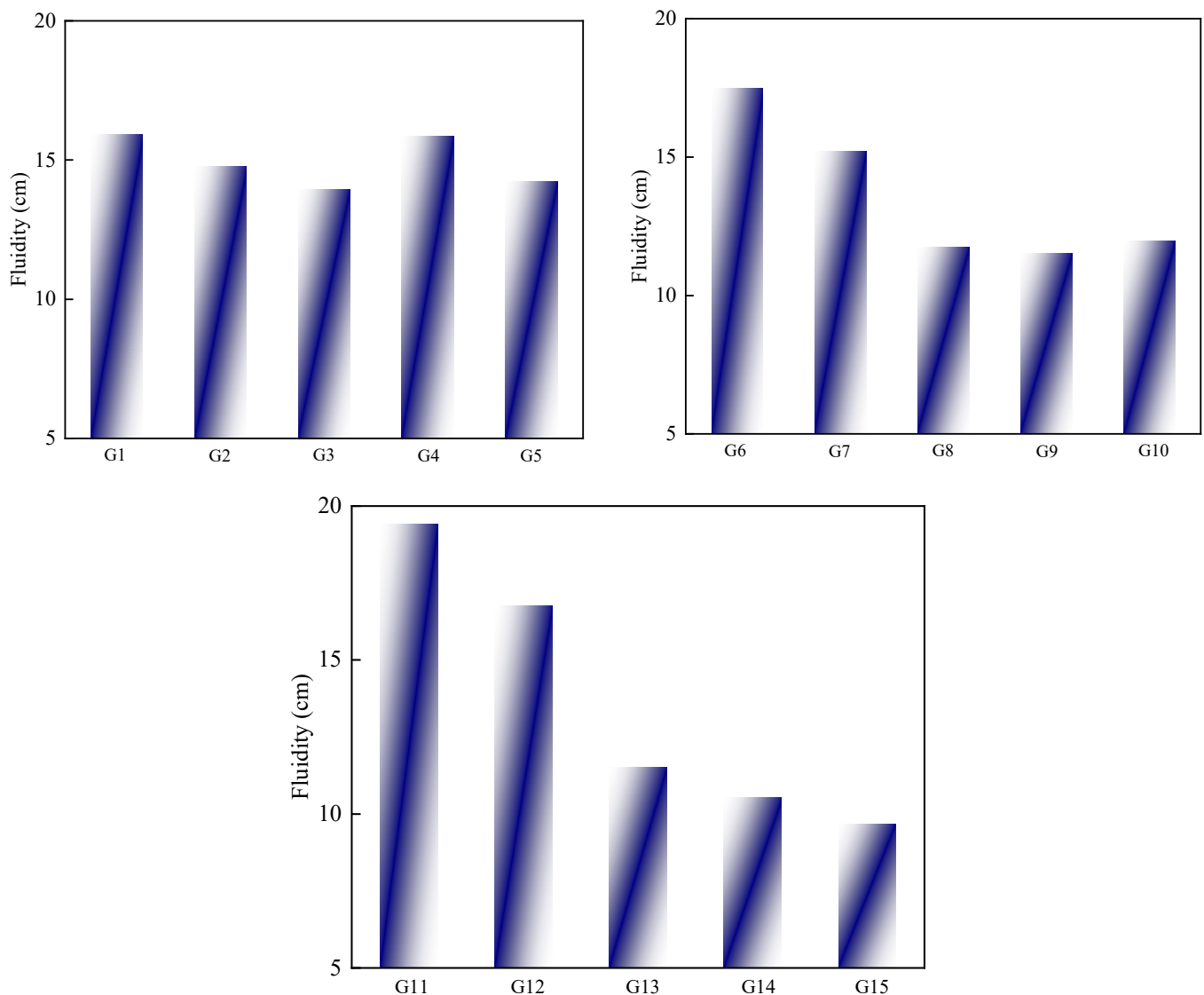


Figure 8. Setting times of grout prepared from a single thermally activated loess.

### 3.3.2. Fluidity Behavior

The change in slurry fluidity when different dosages of mechanically activated loess were prepared for the cement injection slurry is shown in Figure 9. When the dosage of mechanically activated loess was 20%, the fluidity values of the slurry first decreased, then increased, and, finally, decreased again. With increasing grinding time, loess particle size became smaller. The proportion of ultrafine particles increased. When mixed with cement to prepare the slurry, more free water was used to wrap the solid particles. Thus, the interlayer water decreased, and the chances of a solid particle collision increased. The flow resistance increased and the fluidity decreased. When the dosage of mechanically activated loess was 35% or 50%, the fluidity of the slurry rapidly declined and then remained stable or slowly declined. For example, when the dosage reached 35%, due to the grain size of G0 and G10 loess being coarse, the packing density of the slurry packing system decreased with the increase in the adding ratio. The specific surface area of the material was reduced. The number of solid particles in the interlayer water increased. The resistance to flow decreased. The fluidity was elevated. The flow degrees of G0 and G10 were 17.5 cm and 15.53 cm, respectively. However, the particle sizes of G20, G40, and G80 were smaller. Increasing the addition ratio increased the proportion of ultrafine particles, reducing the flow degree [54–56].



**Figure 9.** Flowability of mechanically activated loess for preparing grouting fluids.

The change in the fluidity of the slurry when cement injection slurry was prepared using different dosages of the single heat-activated loess is shown in Figure 10. Regardless of the dosage of the single heat-activated loess, the fluidity of the injection slurry decreased with increasing dosage. For example, when the C400, C550, C700, and C850 dopings reached 20%, the fluidity value of the slurry decreased from 15.01 cm to 13.28 cm. Single heat activated loess has the same raw material grinding time and particle size distribution. The internal structure changes after high temperature calcination. The ultra-fine particles produced upon calcination reduced the fluidity of the slurry. Calcination increased the pozzolanic activity and accelerated the initial hydration, partially affecting the fluidity of the slurry [57–59].

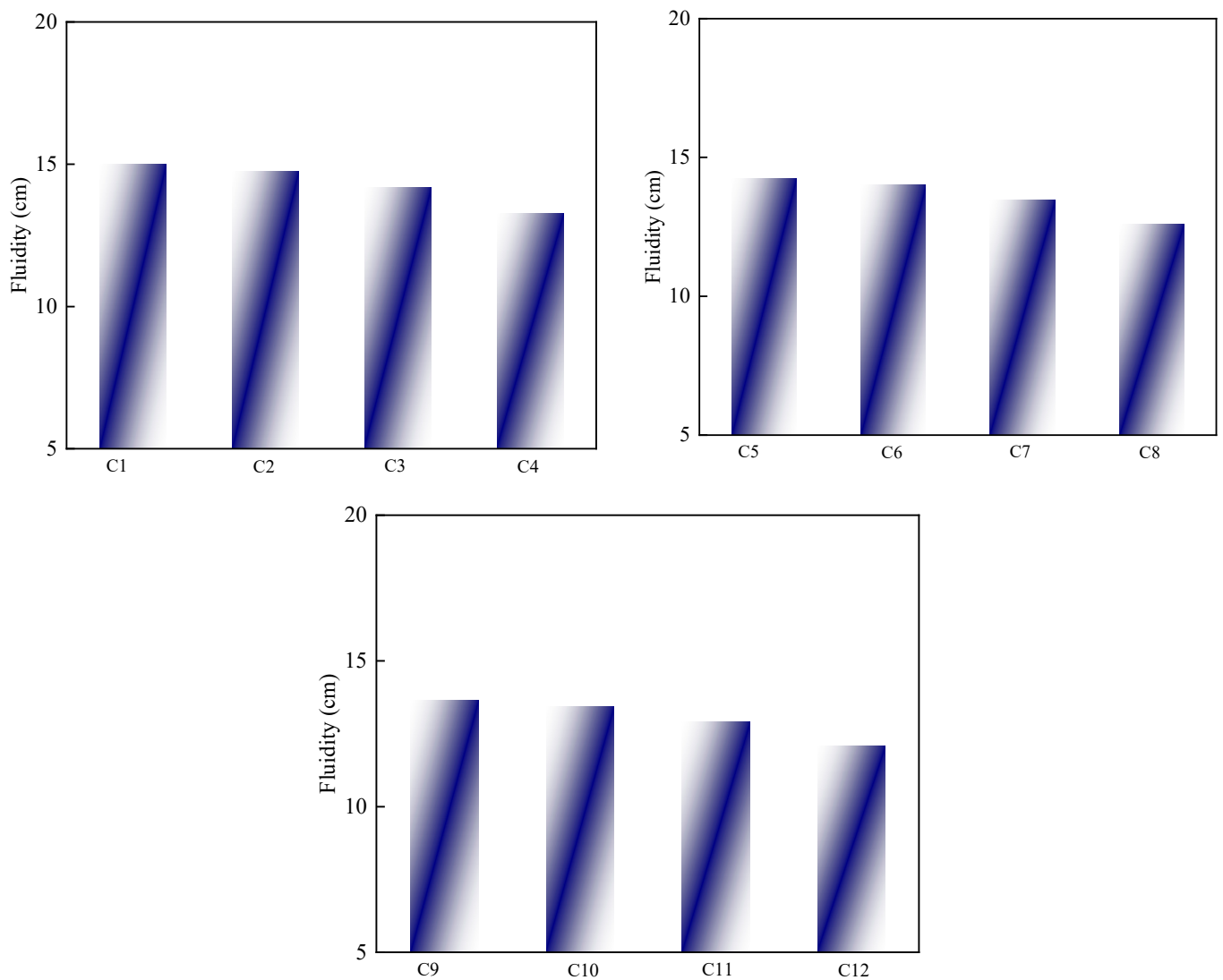


**Figure 10.** Flowability of grouting fluids prepared from a single thermally activated topsoil.

### 3.3.3. UCS and TG Analyses

This section discusses the strengths of hardened grouted materials with the modified loess at different dosages after 3 and 28 days of hydration. The mechanical properties of the hardened materials decreased with cement replacement from 20% to 50% for milled and calcined loess. For example, the UCS value after 28 days of hydration decreased from 16.5 MPa to 8.7 MPa when the admixture of 20 min milled loess increased from 20% to 50%. The UCS value after 28 days of hydration decreased from 21 MPa to 12 MPa when the admixture of the loess calcined at 850 °C increased from 20% to 50%. The other milling times and calcination temperatures studied followed the same pattern [60].

The post-hydration strength first increased and then decreased with increasing grinding time (Figure 11). For example, the highest strength was obtained after the hydration of the loess mixed with cement by grinding for 20 min at a 20% dose. The strength reached 16.5 MPa after 28 days due to the higher specific surface area, which enhanced the filler effect and the pozzolanic reaction and increased hydrate nucleation sites. Grinding activation led to particle pulverization and an increase in the specific surface area until the maximum fineness was obtained. Further grinding did not lead to additional particle refinement. Instead, the agglomeration of submicron particles into porous spherical aggregates occurred. The specific surface area decreased steadily. The agglomeration process was parallel to the extensive decomposition (amorphization) of the kaolinite crystal structure and the recombination of bound water into poorly bound hydroxyl groups. The long-term grinding of environmental conditions led to the adsorption and incorporation of additional atmospheric water [61,62].

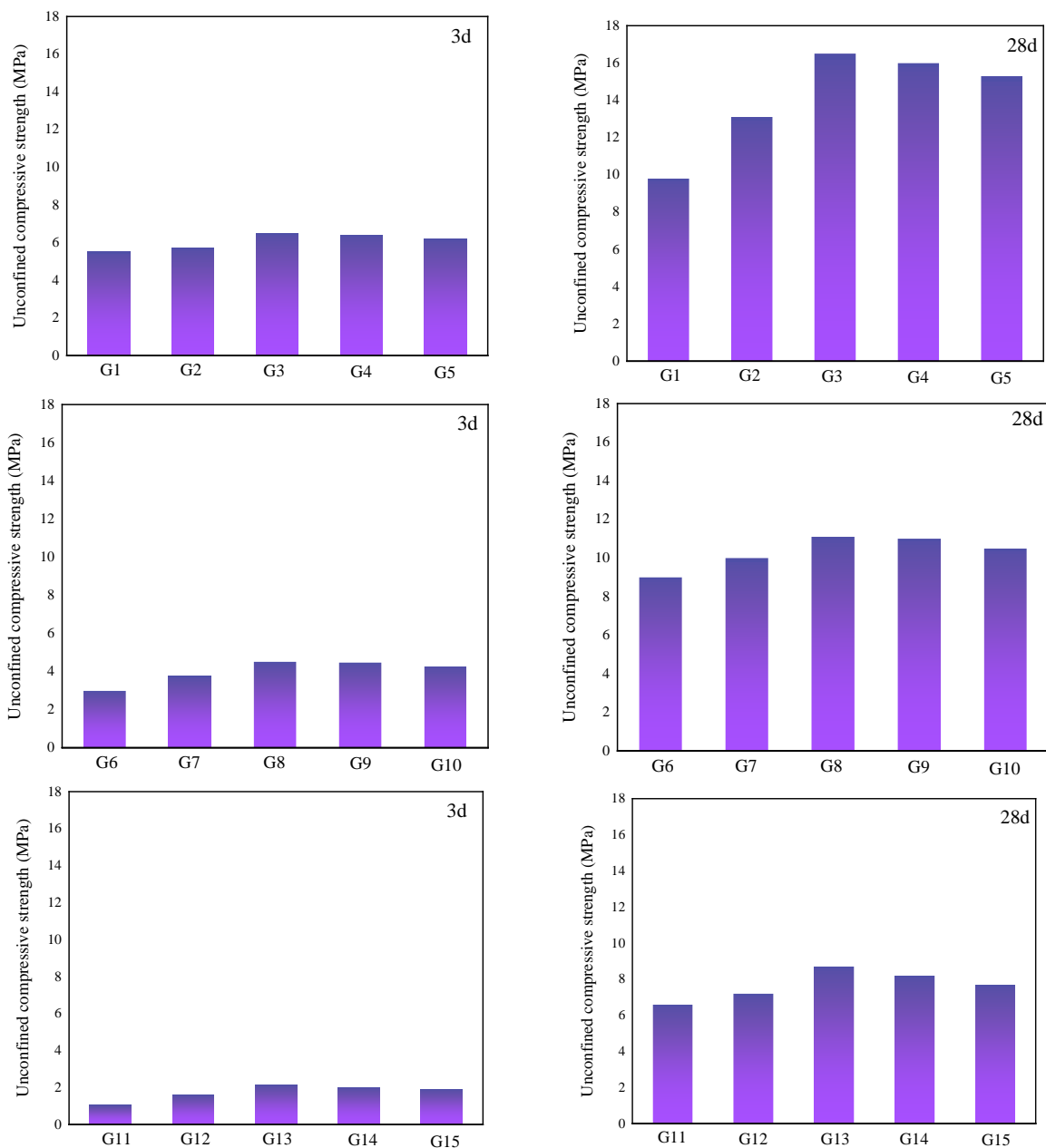


**Figure 11.** Strength of hardened loess mixed with cement in different proportions for different grinding times.

When the temperature was lower, most clay minerals still existed. The lattice adsorbed a certain amount of water, which reduced the contact between gelatinous matter and water. It affected the continuous hydration of the cementitious system and reduced its strength.

The strength of the hydrated solidus increased with increasing calcination temperature at 400 °C–850 °C (Figure 12). For example, the USC values after 3 and 28 days of hydration were 8.5 MPa and 21 MPa, respectively, when the content of loess was 20% at 850 °C. This was primarily because of the increase in the calcination temperature. As the activity of Si and Al increased, the pozzolanic activity of loess also increased (Figure 5). The Si-Al phase underwent a pozzolanic reaction with calcium hydroxide during cement hydration. Parallely, loess with a higher calcination temperature had a higher degree of de-hydroxylation and a larger specific surface area, explaining why it exhibited higher pozzolanic activity, resulting in greater compressive strength [46,63].

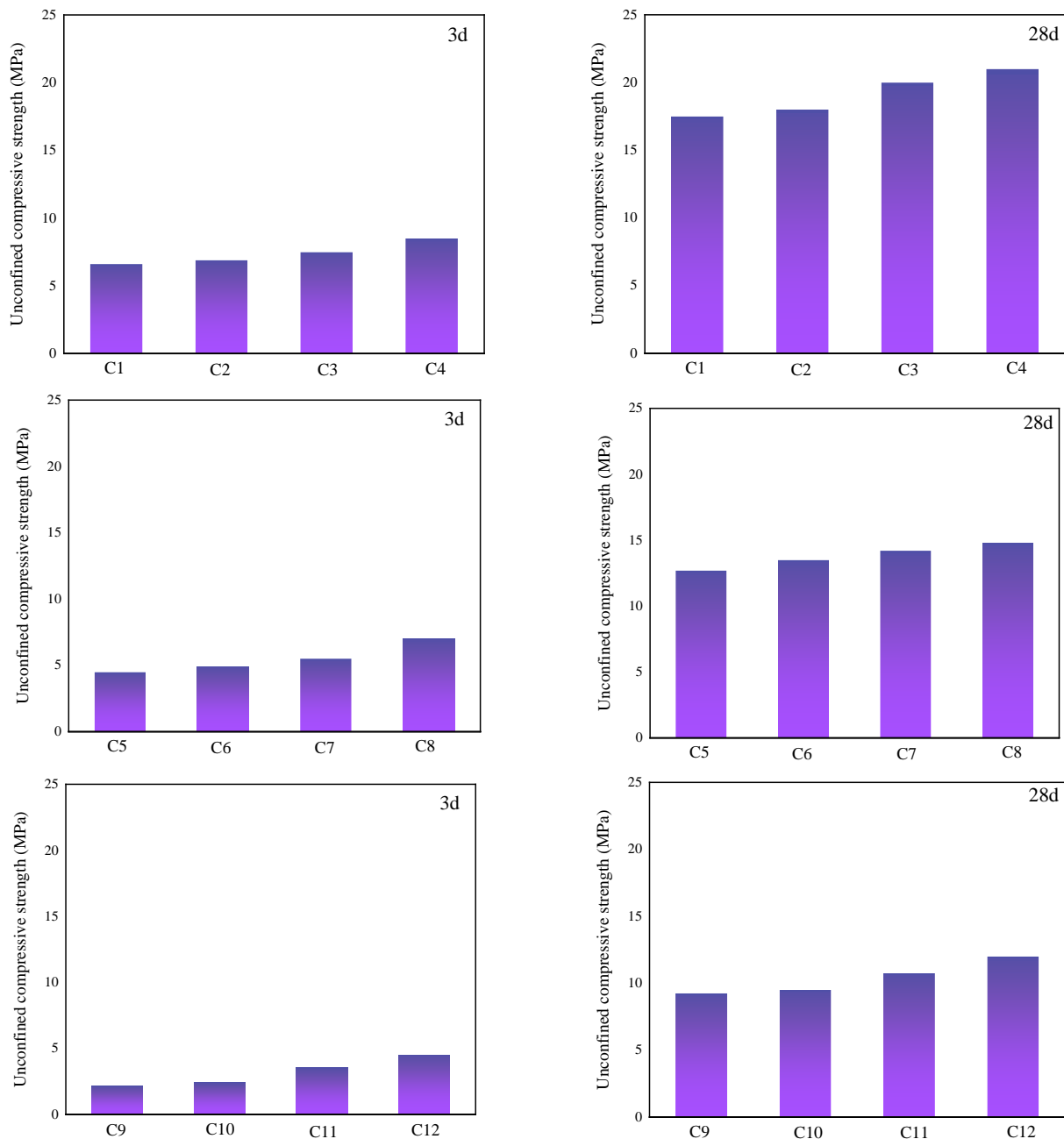


**Figure 12.** Strength at different calcination temperatures of loess mixed with cement in different proportions after hardening.

The heat absorption peak of adsorbed water dehydration broadened as the milling time increased (Figure 13). This water was produced by the mechanical de-hydroxylation of kaolinite and then connected to the newly formed active surface. Owing to the increased defects in the octahedral structure, the endothermic peak of kaolinite de-hydroxylation was obtained at a lower temperature. The decrease in particle size and the disordered structure of kaolinite resulted in the weakening of the binding of OH groups, which controlled the shape and range of de-hydroxylation peaks. For the samples prepared using mechano-chemically treated minerals, a reduction in portlandite (CH) was observed, mainly due to dilution effects [64,65].

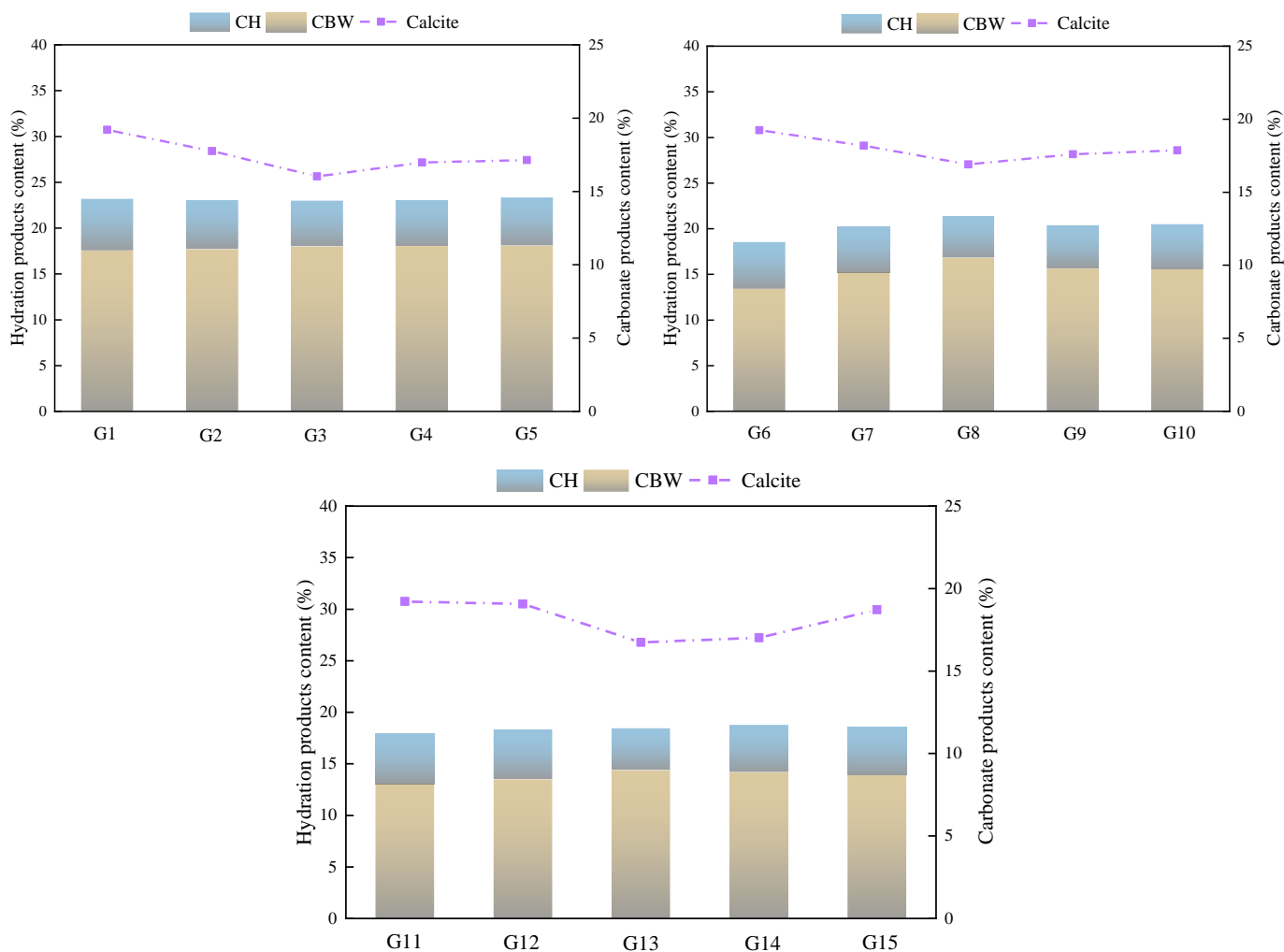


**Figure 13.** Hydration products of loess mixed with cement in different proportions for different grinding times.

The amounts of chemically bound water (CBW), CH, and calcite were calculated using the TG method to study the hydration process of the grouted material hardened in 28 days (Figure 14). The amount of CBW increased as the calcination temperature increased. Due to the higher calcination temperatures, loess has higher pozzolanic activity and could form more C-S-H gels, ettringite, HC, and MC, leading to the high strengths of the hardened samples with high calcination temperatures. As the pozzolanic reaction proceeded, the higher temperature produced less CH [66,67].

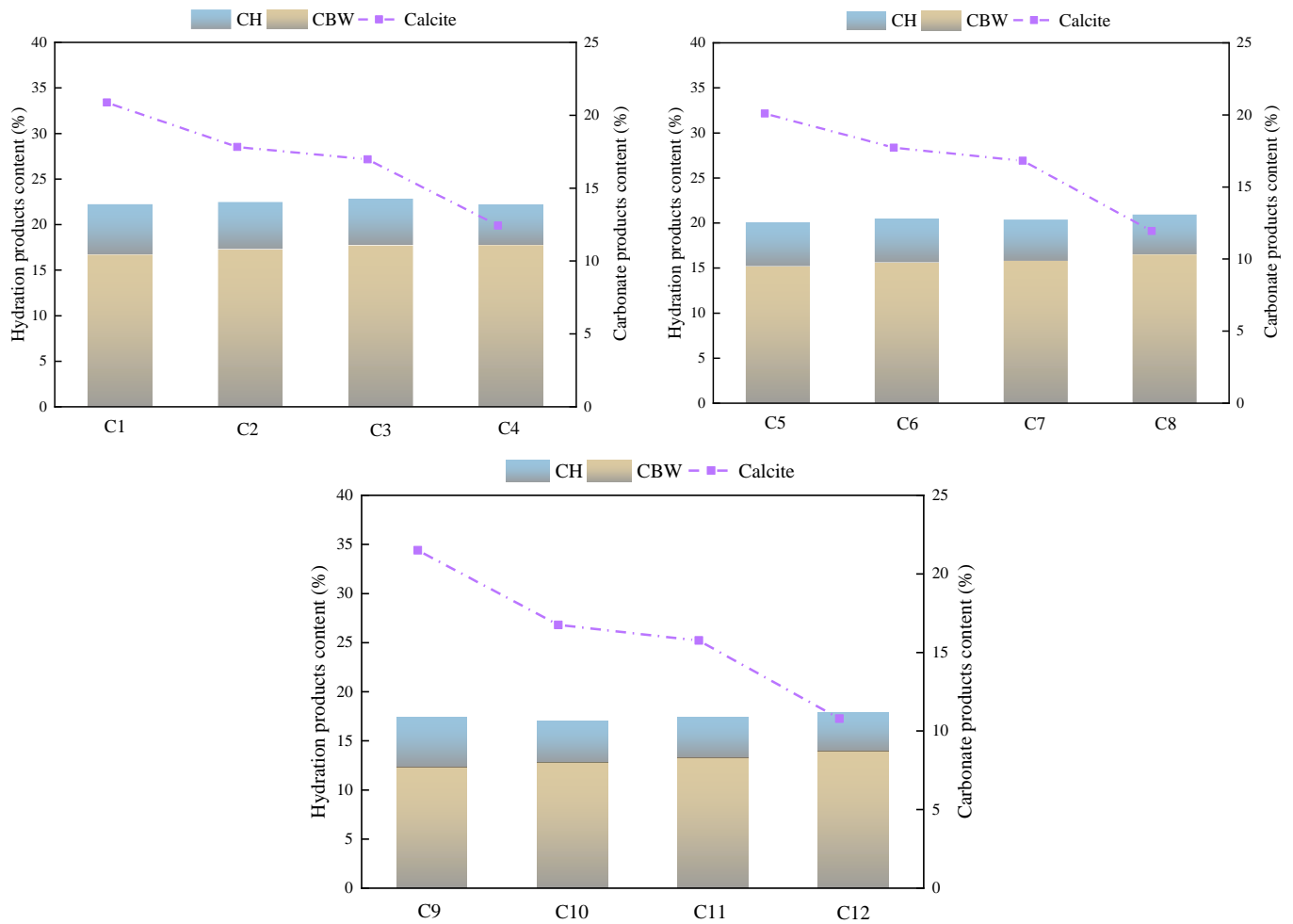


**Figure 14.** Hydration products of loess mixed with cement in different proportions at different calcination temperatures.

The mineral phase of the hydrated binder of calcined loess was analyzed using XRD, and the experimental results are shown in Figure 15. The hydration products of the mixture of calcined loess and cement were primarily CH, ettringite (AFt), calcium silicate hydrate (C-S-H), mono-carboaluminate (Mc), and calcite. Additionally, inert quartz could be observed. The peak value near  $2\theta = 18.1^\circ$  was reduced post-calcination, which belonged to CH. After heat treatment, the reactivity of loess was significantly enhanced and more CH was consumed in the hydration process of the composites. Consistent with the thermal analysis results shown in Figure 14, this effect increased with increasing calcination temperature. With increasing calcination temperature and cement addition ratio, the amount of ettringite and hydrated calcium silicate also increased. During the initial hydration process, sufficient calcite was helpful for Mc formation [68,69].

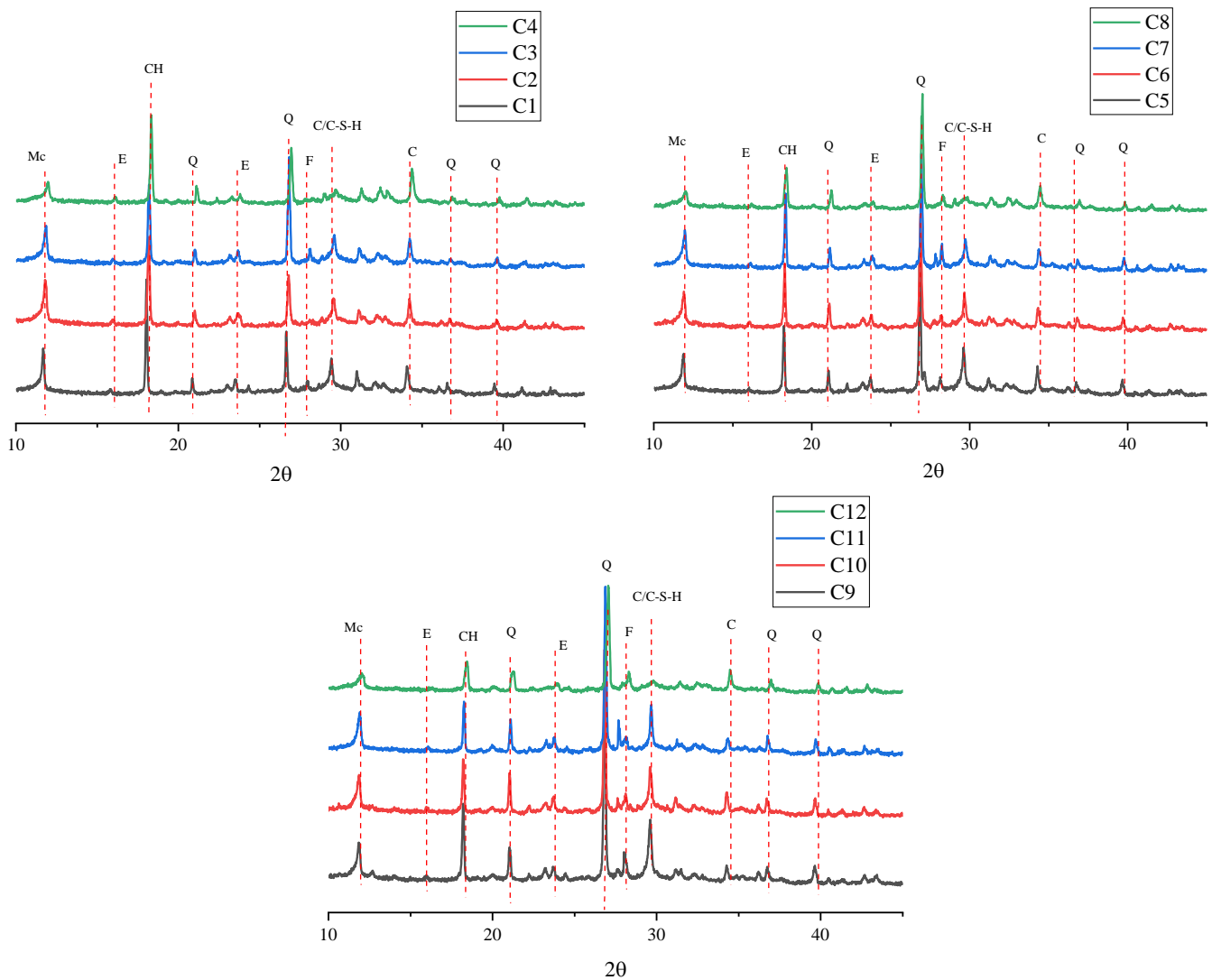


**Figure 15.** XRD patterns of the blended binders hydrated for 28 days (E, Ettringite; Mc, Monocarboaluminate; CH, Portlandite; Q, quartz; C, calcite; F, Feldspars).

#### 4. Conclusions

Supplementary cementitious materials (SCMs) were prepared using the mechano-thermal activation of loess. The activated loess was investigated using XRD, FTIR spectroscopy, and ICP-OES. The grouting materials were also prepared using different cement ratios to investigate their flow, mechanical properties, and hydration evolution. Based on the experimental results, the following conclusions can be drawn:

- (1) Loess decreases in particle size and increases in ultrafine particles with increasing grinding time, which destroys the internal structure of the highly crystalline loess and increases the contact points of the alkaline reaction and the degree of disorder in Si and Al, thereby improving the pozzolanic activity. The increase in ultrafine particles after further grinding leads to agglomeration, forming porous spherical aggregates.
- (2) The pozzolanic activity of modified loess increases with the increase in calcination temperature. At 550 °C, the free and bound water of loess was lost. At 850 °C, anorthite and muscovite decomposed and their peak intensities decreased. The vibrations in the 400–500  $\text{cm}^{-1}$  spectral band indicated that the destruction of the Si–O covalent bond at high temperatures produced Si-phases. The spectral bands of

$\sim 900\text{ cm}^{-1}$  and  $\sim 1400\text{ cm}^{-1}$  corresponded to the vibrations of the C–O bond in  $\text{CO}_3^{2-}$ , indicating that carbonate partially decomposed at  $850\text{ }^\circ\text{C}$ .

- (3) Increasing the grinding time reduces the fluidity and increases the setting time of loess. As an auxiliary cementitious material, this can improve the uniaxial compressive strength. As the calcination temperature increases, the fluidity and setting time decrease. Simultaneously, the pozzolanic activity is improved, which promotes the formation of C–S–H gel and ettringite and increases the compressive strength.

The loess was modified by mechanical grinding and high-temperature calcination respectively by physical and chemical activation. In the future, it can be modified by adding an alkaline activator, increasing the calcium content, and calcining to stimulate its pozzolanic activity. It is also necessary to carry out grouting reinforcement experiments in a coal mine in Shanxi Province to evaluate its applicability. The difference in loess composition in different sedimentary environments and its influence on loess grouting materials should also be studied or a model should be developed to guide the evaluation of loess sources to obtain appropriate mixtures.

**Author Contributions:** Conceptualization, K.W.; Validation, S.Z.; Formal analysis, X.Z.; Data curation, Y.J.; Writing—original draft, H.B. All authors have read and agreed to the published version of the manuscript.

**Funding:** The authors gratefully acknowledge the financial support from the National Natural Science Foundation of China (grant no. 52304148), Youth Project of Shanxi Basic Research Program (grant no. 202203021212262), and the National Science Foundation of China (grant no. 51974194).

**Data Availability Statement:** No new data were created or analyzed in this study.

**Conflicts of Interest:** The authors declare that they have no known competing financial interest or personal relationships that could have appeared to influence the work reported in this paper.

## References

- Korkmaz, A.V. Mechanical activation of diabase and its effect on the properties and microstructure of Portland cement. *Case Stud. Constr. Mater.* **2022**, *16*, e00868. [[CrossRef](#)]
- Baki, V.A.; Ke, X.; Heath, A.; Calabria-Holley, J.; Terzi, C.; Sirin, M. The impact of mechanochemical activation on the physico-chemical properties and pozzolanic reactivity of kaolinite, muscovite and montmorillonite. *Cem. Concr. Res.* **2022**, *162*, 106962. [[CrossRef](#)]
- Donatello, S.; Freeman-Pask, A.; Tyrer, M.; Cheeseman, C.R. Effect of milling and acid washing on the pozzolanic activity of incinerator sewage sludge ash. *Cem. Concr. Compos.* **2010**, *32*, 54–61. [[CrossRef](#)]
- Tole, I.; Delogu, F.; Qoku, E.; Habermehl-Cwirzen, K.; Cwirzen, A. Enhancement of the pozzolanic activity of natural clays by mechanochemical activation. *Constr. Build. Mater.* **2022**, *352*, 128739. [[CrossRef](#)]
- Yao, G.; Liu, Q.; Wang, J.; Wu, P.; Lyu, X. Effect of mechanical grinding on pozzolanic activity and hydration properties of siliceous gold ore tailings. *J. Clean. Prod.* **2019**, *217*, 12–21. [[CrossRef](#)]
- Yao, G.; Wang, Z.; Yao, J.; Cong, X.; Anning, C.; Lyu, X. Pozzolanic activity and hydration properties of feldspar after mechanical activation. *Powder Technol.* **2021**, *383*, 167–174. [[CrossRef](#)]
- Yao, G.; Cui, T.; Zhang, J.; Wang, J.; Lyu, X. Effects of mechanical grinding on pozzolanic activity and hydration properties of quartz. *Adv. Powder Technol.* **2020**, *31*, 4500–4509. [[CrossRef](#)]
- Sun, X.; Zhao, Y.; Tian, Y.; Wu, P.; Guo, Z.; Qiu, J.; Xing, J.; Xiaowei, G. Modification of high-volume fly ash cement with metakaolin for its utilization in cemented paste backfill: The effects of metakaolin content and particle size. *Powder Technol.* **2021**, *393*, 539–549. [[CrossRef](#)]
- Andrić, L.; Terzić, A.; Aćimović-Pavlović, Z.; Pavlović, L.; Petrov, M. Comparative kinetic study of mechanical activation process of mica and talc for industrial application. *Compos. Part B Eng.* **2014**, *59*, 181–190. [[CrossRef](#)]
- Yao, G.; Zang, H.; Wang, J.; Wu, P.; Qiu, J.; Lyu, X. Effect of Mechanical Activation on the Pozzolanic Activity of Muscovite. *Clays Clay Miner.* **2019**, *67*, 209–216. [[CrossRef](#)]
- Mitrović, A.; Zdujić, M. Preparation of pozzolanic addition by mechanical treatment of kaolin clay. *Int. J. Miner. Process.* **2014**, *132*, 59–66. [[CrossRef](#)]
- Zunino, F.; Scrivener, K. Increasing the kaolinite content of raw clays using particle classification techniques for use as supplementary cementitious materials. *Constr. Build. Mater.* **2020**, *244*, 118335. [[CrossRef](#)]
- Tole, I.; Habermehl-Cwirzen, K.; Cwirzen, A. Mechanochemical activation of natural clay minerals: An alternative to produce sustainable cementitious binders—Review. *Mineral. Petrol.* **2019**, *113*, 449–462. [[CrossRef](#)]

14. Neißer-Deiters, A.; Scherb, S.; Beuntner, N.; Thienel, K.-C. Influence of the calcination temperature on the properties of a mica mineral as a suitability study for the use as SCM. *Appl. Clay Sci.* **2019**, *179*, 105168. [[CrossRef](#)]
15. Irassar, E.F.; Bonavetti, V.L.; Castellano, C.C.; Trezza, M.A.; Rahhal, V.F.; Cordoba, G.; Lemma, R. Calcined illite-chlorite shale as supplementary cementing material: Thermal treatment, grinding, color and pozzolanic activity. *Appl. Clay Sci.* **2019**, *179*, 105143. [[CrossRef](#)]
16. Hao, R.; Li, X.; Xu, P.; Liu, Q. Thermal activation and structural transformation mechanism of kaolinitic coal gangue from Jungar coalfield, Inner Mongolia, China. *Appl. Clay Sci.* **2022**, *223*, 106508. [[CrossRef](#)]
17. Buchwald, A.; Hohmann, M.; Posern, K.; Brendler, E. The suitability of thermally activated illite/smectite clay as raw material for geopolymer binders. *Appl. Clay Sci.* **2009**, *46*, 300–304. [[CrossRef](#)]
18. Rakhimov, R.Z.; Rakhimova, N.R.; Gaifullin, A.R.; Morozov, V.P. Properties of Portland cement pastes enriched with addition of calcined marl. *J. Build. Eng.* **2017**, *11*, 30–36. [[CrossRef](#)]
19. Sun, T.; Ge, K.; Wang, G.; Geng, H.; Shui, Z.; Cheng, S.; Chen, M. Comparing pozzolanic activity from thermal-activated water-washed and coal-series kaolin in Portland cement mortar. *Constr. Build. Mater.* **2019**, *227*, 117092. [[CrossRef](#)]
20. Liu, Y.; Lei, S.; Lin, M.; Xia, Z.; Pei, Z.; Li, B. Influence of calcined coal-series kaolin fineness on properties of cement paste and mortar. *Constr. Build. Mater.* **2018**, *171*, 558–565. [[CrossRef](#)]
21. Scrivener, K.; Martirena, F.; Bishnoi, S.; Maity, S. Calcined clay limestone cements (LC3). *Cem. Concr. Res.* **2018**, *114*, 49–56. [[CrossRef](#)]
22. Wan, Q.; Rao, F.; Song, S. Reexamining calcination of kaolinite for the synthesis of metakaolin geopolymers—Roles of dehydroxylation and recrystallization. *J. Non-Cryst. Solids* **2017**, *460*, 74–80. [[CrossRef](#)]
23. Tironi, A.; Trezza, M.A.; Scian, A.N.; Irassar, E.F. Kaolinitic calcined clays: Factors affecting its performance as pozzolans. *Constr. Build. Mater.* **2012**, *28*, 276–281. [[CrossRef](#)]
24. Claverie, M.; Martin, F.; Tardy, J.P.; Cyr, M.; De Parseval, P.; Grauby, O.; Le Roux, C. Structural and chemical changes in kaolinite caused by flash calcination: Formation of spherical particles. *Appl. Clay Sci.* **2015**, *114*, 247–255. [[CrossRef](#)]
25. Liu, Y.; Lei, S.; Lin, M.; Li, Y.; Ye, Z.; Fan, Y. Assessment of pozzolanic activity of calcined coal-series kaolin. *Appl. Clay Sci.* **2017**, *143*, 159–167. [[CrossRef](#)]
26. Xu, X.; Lao, X.; Wu, J.; Zhang, Y.; Xu, X.; Li, K. Microstructural evolution, phase transformation, and variations in physical properties of coal series kaolin powder compact during firing. *Appl. Clay Sci.* **2015**, *115*, 76–86. [[CrossRef](#)]
27. Zhang, Y.; Xu, L.; Seetharaman, S.; Liu, L.; Wang, X.; Zhang, Z. Effects of chemistry and mineral on structural evolution and chemical reactivity of coal gangue during calcination: Towards efficient utilization. *Mater. Struct.* **2014**, *48*, 2779–2793. [[CrossRef](#)]
28. Lee, V.-G.; Yeh, T.-H. Sintering effects on the development of mechanical properties of fired clay ceramics. *Mater. Sci. Eng. A* **2008**, *485*, 5–13. [[CrossRef](#)]
29. Cheng, S.; Ge, K.; Sun, T.; Shui, Z.; Chen, X.; Lu, J.-X. Pozzolanic activity of mechanochemically and thermally activated coal-series kaolin in cement-based materials. *Constr. Build. Mater.* **2021**, *299*, 123972. [[CrossRef](#)]
30. Vizcayno, C.; de Gutiérrez, R.M.; Castello, R.; Rodríguez, E.; Guerrero, C.E. Pozzolan obtained by mechanochemical and thermal treatments of kaolin. *Appl. Clay Sci.* **2010**, *49*, 405–413. [[CrossRef](#)]
31. Guo, W.; Li, D.; Chen, J.; Yang, N. Structure and pozzolanic activity of calcined coal gangue during the process of mechanical activation. *J. Wuhan Univ. Technol. Mater. Sci. Ed.* **2009**, *24*, 326–329. [[CrossRef](#)]
32. Ilić, B.; Radonjanin, V.; Malešev, M.; Zdujić, M.; Mitrović, A. Effects of mechanical and thermal activation on pozzolanic activity of kaolin containing mica. *Appl. Clay Sci.* **2016**, *123*, 173–181. [[CrossRef](#)]
33. Souri, A.; Kazemi-Kamyab, H.; Snellings, R.; Naghizadeh, R.; Golestani-Fard, F.; Scrivener, K. Pozzolanic activity of mechanochemically and thermally activated kaolins in cement. *Cem. Concr. Res.* **2015**, *77*, 47–59. [[CrossRef](#)]
34. Zhang, S.; Ren, F.; Zhao, Y.; Qiu, J.; Guo, Z. The effect of stone waste on the properties of cemented paste backfill using alkali-activated slag as binder. *Constr. Build. Mater.* **2021**, *283*, 122686. [[CrossRef](#)]
35. Sonebi, M.; Lachemi, M.; Hossain, K.M.A. Optimisation of rheological parameters and mechanical properties of superplasticised cement grouts containing metakaolin and viscosity modifying admixture. *Constr. Build. Mater.* **2013**, *38*, 126–138. [[CrossRef](#)]
36. Singh, M.; Garg, M. Reactive pozzolana from Indian clays—Their use in cement mortars. *Cem. Concr. Res.* **2006**, *36*, 1903–1907. [[CrossRef](#)]
37. Paiva, H.; Velosa, A.; Cachim, P.; Ferreira, V.M. Effect of metakaolin dispersion on the fresh and hardened state properties of concrete. *Cem. Concr. Res.* **2012**, *42*, 607–612. [[CrossRef](#)]
38. Cassagnabère, F.; Diederich, P.; Mouret, M.; Escadeillas, G.; Lachemi, M. Impact of metakaolin characteristics on the rheological properties of mortar in the fresh state. *Cem. Concr. Compos.* **2013**, *37*, 95–107. [[CrossRef](#)]
39. Xu, J.; Zhang, L.; Li, Y.; Li, Z.; Zhao, Y. Mechanical, mineralogical, and microstructural characterization of collapsible loess cured by NaOH solution. *Constr. Build. Mater.* **2024**, *421*, 135678. [[CrossRef](#)]
40. Liu, Y.; Tang, C.; Wen, J.; Guo, H.; Fan, H. Mechanical characterization and water stability of loess improved by bio-based materials: An eco-friendly approach. *Sci. Total Environ.* **2024**, *921*, 171111. [[CrossRef](#)]
41. Zhang, Y.; Liu, B.; Gu, X.; Nehdi, M.L.; Zhang, L.V. Mechanochemical activation of iron ore tailing-based ternary supplementary cementitious materials. *Constr. Build. Mater.* **2022**, *346*, 128420. [[CrossRef](#)]

42. Chen, B.; Pang, L.; Zhou, Z.; Chang, Q.; Fu, P. Study on the activation mechanism and hydration properties of gold tailings activated by mechanical-chemical-thermal coupling. *J. Build. Eng.* **2022**, *48*, 104014. [[CrossRef](#)]
43. Li, Z.; Gao, Y.; Zhang, J.; Zhang, C.; Chen, J.; Liu, C. Effect of particle size and thermal activation on the coal gangue based geopolymer. *Mater. Chem. Phys.* **2021**, *267*, 124657. [[CrossRef](#)]
44. Wang, H.; Liu, X.; Zhang, Z. Pozzolanic activity evaluation methods of solid waste: A review. *J. Clean. Prod.* **2023**, *402*, 136783. [[CrossRef](#)]
45. Zhao, Y.; Qiu, J.; Guo, Z.; Zhang, S.; Wu, P.; Sun, X. Activation the hydration properties of illite-containing tailings to prepare a binder for cemented paste backfill. *Constr. Build. Mater.* **2022**, *318*, 125989. [[CrossRef](#)]
46. Qiu, Z.; Bao, S.; Zhang, Y.; Huang, M.; Lin, C.; Huang, X.; Chen, Y.; Ping, Y. Effect of Portland cement on the properties of geopolymers prepared from granite powder and fly ash by alkali-thermal activation. *J. Build. Eng.* **2023**, *76*, 107363. [[CrossRef](#)]
47. Yanguatin, H.; Ramírez, J.H.; Tironi, A.; Tobón, J.I. Effect of thermal treatment on pozzolanic activity of excavated waste clays. *Constr. Build. Mater.* **2019**, *211*, 814–823. [[CrossRef](#)]
48. Derouiche, R.; Baklouti, S. Phosphoric acid based geopolymerization: Effect of the mechanochemical and the thermal activation of the kaolin. *Ceram. Int.* **2021**, *47*, 13446–13456. [[CrossRef](#)]
49. d’Azevedo, C.A.; de Assis, T.C.; Silva, F.A.N.G.; Siqueira, J.M.; Garrido, F.M.S.; Medeiros, M.E. Preparation of  $\alpha$ -cordierite through mechanochemical activation of  $MgO-Al_2O_3-SiO_2$  ternary system. *Ceram. Int.* **2022**, *48*, 18658–18666. [[CrossRef](#)]
50. Jin, Z.; Wang, L.; Su, Y.; He, X.; Ma, B.; Wang, Y.; Li, Y.; Qi, H.; Wang, B. Effect of different retarders on setting time and mechanical properties of hemihydrate phosphogypsum-calcium sulfoaluminate cement composite binder. *Constr. Build. Mater.* **2024**, *411*, 134339. [[CrossRef](#)]
51. Ng, Y.L.; Aldahdooh, M.A.A.; Alazaiza, M.Y.D.; Bashir, M.J.K.; Chok, V.S.; Ng, C.A. Influence of alum sludge ash and ground granulated blast furnace slag on properties of cement mortar. *Clean. Eng. Technol.* **2022**, *6*, 100376. [[CrossRef](#)]
52. Perná, I.; Hanzlíček, T. The setting time of a clay-slag geopolymer matrix: The influence of blast-furnace-slag addition and the mixing method. *J. Clean. Prod.* **2016**, *112*, 1150–1155. [[CrossRef](#)]
53. Ouyang, S.; Huang, Y.; Wu, L.; Yin, W.; Yang, X.; Wang, J.; Wang, G.; Li, J.; Lei, Y. Effects of chlorides on setting time, hydration heat and hydration products of fresh slurry of cemented paste backfill. *Case Stud. Constr. Mater.* **2022**, *17*, e01462. [[CrossRef](#)]
54. Guo, Z.; Qiu, J.; Jiang, H.; Zhang, S.; Ding, H. Improving the performance of superfine-tailings cemented paste backfill with a new blended binder. *Powder Technol.* **2021**, *394*, 149–160. [[CrossRef](#)]
55. Hu, Y.; Li, K.; Zhang, B.; Han, B. Effect of nano- $SiO_2$  on mechanical properties, fluidity, and microstructure of superfine tailings cemented paste backfill. *Mater. Today Sustain.* **2023**, *24*, 100490. [[CrossRef](#)]
56. Dong, D.; Huang, Y.; Pei, Y.; Zhang, X.; Cui, N.; Zhao, P.; Hou, P.; Lu, L. Effect of spherical silica fume and fly ash on the rheological property, fluidity, setting time, compressive strength, water resistance and drying shrinkage of magnesium ammonium phosphate cement. *J. Build. Eng.* **2023**, *63*, 105484. [[CrossRef](#)]
57. Shao, C.; Liu, L.; Zhang, X.; Xie, L.; Ruan, S.; Zhu, M.; Yang, P.; Liu, D. Influence of internal and external factors on the fluidity of modified magnesium slag-based backfill materials. *J. Environ. Chem. Eng.* **2024**, *12*, 111867. [[CrossRef](#)]
58. Kaze, C.R.; Adesina, A.; Lecomte-Nana, G.L.; Alomayri, T.; Kamseu, E.; Melo, U.C. Alkali-activated laterite binders: Influence of silica modulus on setting time, Rheological behaviour and strength development. *Clean. Eng. Technol.* **2021**, *4*, 100175. [[CrossRef](#)]
59. Kaze, C.R.; Lecomte-Nana, G.L.; Adesina, A.; Nemaleu, J.G.D.; Kamseu, E.; Chinje Melo, U. Influence of mineralogy and activator type on the rheology behaviour and setting time of laterite based geopolymer paste. *Cem. Concr. Compos.* **2022**, *126*, 104345. [[CrossRef](#)]
60. Hernández-Ramos, S.M.; Trejo-Arroyo, D.L.; Cholicó-González, D.F.; Rodríguez-Torres, G.M.; Zárate-Medina, J.; Vega-Azamar, R.E.; León-Patiño, C.A.; Ortiz-Lara, N. Characterization and effect of mechanical and thermal activation in mining tailings for use as supplementary cementitious material. *Case Stud. Constr. Mater.* **2024**, *20*, e02770. [[CrossRef](#)]
61. Makó, É.; Óze, C. The effects of silica fume and diatomaceous earth on the mechanochemical activation and pozzolanic activity of kaolin. *Appl. Clay Sci.* **2022**, *228*, 106636. [[CrossRef](#)]
62. Hosseini, S.; Brake, N.A.; Nikookar, M.; Günaydin-Şen, Ö.; Snyder, H.A. Mechanochemically activated bottom ash-fly ash geopolymer. *Cem. Concr. Compos.* **2021**, *118*, 103976. [[CrossRef](#)]
63. Bullerjahn, F.; Zajac, M.; Pekarkova, J.; Nied, D. Novel SCM produced by the co-calcination of aluminosilicates with dolomite. *Cem. Concr. Res.* **2020**, *134*, 106083. [[CrossRef](#)]
64. De Weerd, K.; Haha, M.B.; Le Saout, G.; Kjellsen, K.O.; Justnes, H.; Lothenbach, B. Hydration mechanisms of ternary Portland cements containing limestone powder and fly ash. *Cem. Concr. Res.* **2011**, *41*, 279–291. [[CrossRef](#)]
65. Wu, M.; Zhang, Y.; Jia, Y.; She, W.; Liu, G.; Yang, Y.; Rong, Z.; Sun, W. The influence of chemical admixtures on the strength and hydration behavior of lime-based composite cementitious materials. *Cem. Concr. Compos.* **2019**, *103*, 353–364. [[CrossRef](#)]
66. Wang, H.; Hou, P.; Li, Q.; Adu-Amankwah, S.; Chen, H.; Xie, N.; Zhao, P.; Huang, Y.; Wang, S.; Cheng, X. Synergistic effects of supplementary cementitious materials in limestone and calcined clay-replaced slag cement. *Constr. Build. Mater.* **2021**, *282*, 122648. [[CrossRef](#)]
67. Zhang, D.; Zhang, S.; Huang, B.; Yang, Q.; Li, J. Comparison of mechanical, chemical, and thermal activation methods on the utilisation of recycled concrete powder from construction and demolition waste. *J. Build. Eng.* **2022**, *61*, 105295. [[CrossRef](#)]

68. Zhang, S.; Ren, F.; Ding, H.; Qiu, J.; Tian, Y.; Liu, N. Recycling aluminum dross as a mineral admixture in CaO-activated superfine slag. *Constr. Build. Mater.* **2021**, *279*, 122434. [[CrossRef](#)]
69. Kaze, C.R.; Beleuk à Mougam, L.M.; Sontia Metekong, J.V.; Alomayri, T.S.; Naghizadeh, A.; Tchadjie, L. Thermal behaviour, microstructural changes and mechanical properties of alkali-activated volcanic scoria-fired waste clay brick blends. *Dev. Built Environ.* **2023**, *14*, 100153. [[CrossRef](#)]

**Disclaimer/Publisher's Note:** The statements, opinions and data contained in all publications are solely those of the individual author(s) and contributor(s) and not of MDPI and/or the editor(s). MDPI and/or the editor(s) disclaim responsibility for any injury to people or property resulting from any ideas, methods, instructions or products referred to in the content.